PAPER

Infiltration and recharge dynamics in the Nubian Sandstone Aquifer System of northern Chad

Marie-Louise A. Vogt[1] · François Zwahlen[1] · Sebastián Pera[2] · Hamza Brahim Mahamat[3] · Daniel Hunkeler[1] · Philip Brunner[1]

Abstract

The Nubian Sandstone Aquifer System (NSAS) is one of the world's largest fossil groundwater resources. In northern Chad, notably in the areas of the Tibesti and Ennedi mountains, precipitation occurs seasonally with rates up to 150 mm year^{-1}. This precipitation could lead to diffuse recharge, as well as concentrated recharge along the episodically flooded wadis. Although it is clear that infiltration occurs under flooded areas, it is unknown if and to what extent the infiltration can recharge groundwater. This study combines remote sensing data on precipitation, evapotranspiration, and the temporal and spatial dynamics of the flooded areas with chemical and stable isotopic data from groundwater and surface water sampled between 2013 and 2016. The combination of these data shows that (1) the only area where diffuse recharge occurs is in the southern area of the Ennedi mountains, where concentrated recharge through the wadis occurs concurrently during the month of August, and (2) southeast of the Tibesti and north of the Ennedi mountains, only concentrated recharge occurs. The length of the flooded areas and thus the spatial extent of concentrated recharge varies significantly from year to year and can last up to 3 months. The study has shown that modern recharge does occur in northern Chad, but to a very limited extent, both in space and time. This means that achieving sustainable management of this renewable resource can only be considered through rigorous quantitative assessments. Furthermore, these findings have important implications for future studies on the regional dynamics of the NSAS.

✉ Marie-Louise A. Vogt
marielouise@hydrodynamic.ch

François Zwahlen
francois.zwahlen@unine.ch

Sebastián Pera
sebastian.pera@supsi.ch

Hamza Brahim Mahamat
hbrahim10@gmail.com

Daniel Hunkeler
daniel.hunkeler@unine.ch

Philip Brunner
philip.brunner@unine.ch

1   Centre d'Hydrogéologie et Géothermie, University of Neuchâtel, rue Emile-Argand 11, 2000 Neuchâtel, Switzerland

2   Istituto Scienze della Terra, Scuola Universitaria della Svizzera Italiana, Mendrisio, Switzerland

3   Université Polytechnique de Mongo, Mongo, Chad

Introduction

The Nubian Sandstone Aquifer System (NSAS) is one of the world's largest aquifer systems, with a total surface of 2.2 million km^2 (CEDARE 2002), shared between the countries of Libya, Egypt, Sudan, and Chad (Fig. 1). The large basin is subdivided into subbasins Dakhla, Northern Sudan Platform and Kufrah. The Kufrah basin extends from northern Chad to central Libya, covering a surface area of 400,000 km^2 and with estimated groundwater storage of 25,000 km^3 (Said and El-Mehdi 2000). The NSAS lies in an arid to hyper-arid environment. Groundwater dating based on ^{14}C measurements showed that most of the groundwater is fossil water (Münnich and Vogel 1963; Klitzsch et al. 1976; Edmunds and Wright 1979; Sonntag et al. 1982; Swailem et al. 1983) and that considerable amounts of recharge occurred during the humid pluvial periods of the Pleistocene to the Holocene (paleorecharge).
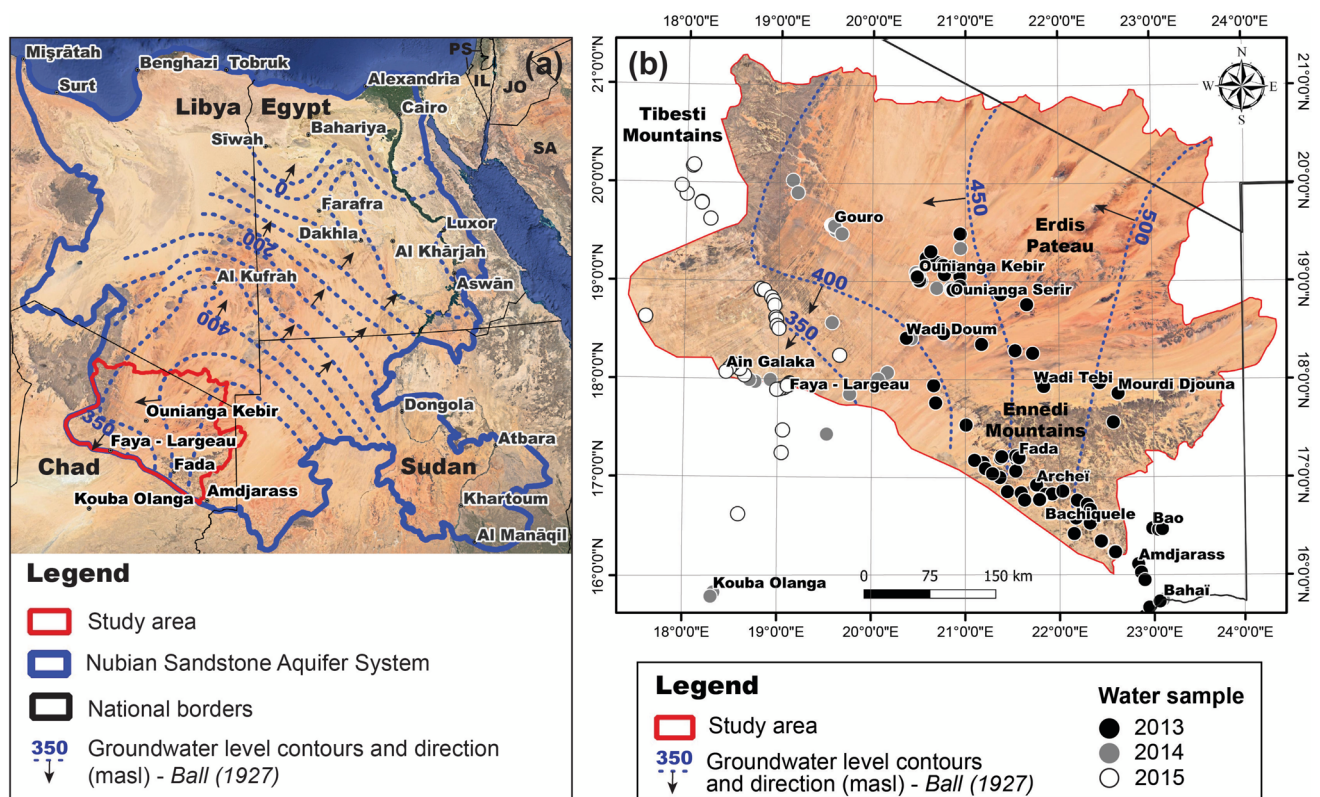
Fig. 1 **a** Extent and regional groundwater flow system of the Nubian Sandstone Aquifer System (NSAS). Blue dashed lines indicate the groundwater level measured [m above sea level (masl)] and interpreted by Ball (1927) (compiled after Gossel et al. 2004). The red line shows the study area (total surface area 2.39 10^5 km²). **b** Zoom to the study area. The mountain ranges of northern Chad are the Ennedi, Erdis, Tibesti. The background images were obtained from Google Earth

While some hydrogeological conceptual models of the entire system are available (e.g. Pallas 1980; Wright et al. 1982; Mahamoud 1986; Hesse et al. 1987), the deep geology remains poorly understood, particularly for northern Chad (Williams 1966; Vogt 2019). Concerning modern recharge, the current state of research is incomplete. In northern Sudan and Egypt (Muller and Haynes 1984; El Bakri et al. 1991; Vrbka and Thorweihe 1993; Suckow et al. 1993; Sturchio et al. 1996; Sultan et al. 1997), stable isotopes (^{18}O, ^{2}H) have been used to differentiate the modern recharged groundwater from the fossil groundwater, because of the characteristic depleted stable isotopic signature of groundwater recharged during the Pleistocene, compared to modern precipitation (Edmunds 2009; Abouelmagd et al. 2012). The region of northern Chad has so far not been investigated with regard to recharge and recharge mechanisms. The region is large and difficult to access and no ground-based climatic, hydrologic or hydrogeologic monitoring is currently being performed. There are, however, several indications that modern recharge could indeed occur in this region:

1. The mountainous regions of northern Chad, notably the Tibesti mountains—3,400 m above sea level (masl)—

to the west and the Ennedi mountains (1,300 masl) to the east and south-east capture higher rates of annual precipitation (up to 100–150 mm year^{-1}, compared to the central flat areas with < 30 mm year^{-1}). Given the higher precipitation rates in the region, groundwater recharge could directly occur via infiltrating precipitation (diffuse recharge). Another potential mechanism for modern recharge could be through infiltration under the periodically flooded wadis (concentrated recharge). Wadis are temporarily flooded rivers, which emerge during the rainy season and recede once the rainy season is over. Studies from the *Geographisches Institutes der Freien Universität Berlin* between 1960 to 1980, and from the *Office de la Recherche Scientifique et Technique d'Outre-Mer* between the 1950s and 1960s, documented the temporal flooding of the wadis in northern Chad. ORSTOM (1962) could show that the flooded extent of wadis in the Ennedi mountains is influenced by the precipitation rates. However, it remains unclear to what extent the flooding of the wadis effectively contributes to groundwater recharge.

2. Field-based water level depth measurements dating from 1927 (Ball 1927) show higher hydraulic heads in this

region (see contour lines in Fig. 1), which could be an indication of modern recharge. However, these data are old and the elevated hydraulic heads must not necessarily only be related to the occurrence of modern recharge.

3. Numerical modelling studies of the entire system (Heinl and Brinkmann 1989; Gossel et al. 2004; Sefelnasr et al. 2015; Voss and Soliman 2014) conceptualize recharge in different ways. Gossel et al. (2004) mentioned that they assigned "*a few millimetres per year of recharge on the highland at the southern edge of the model area and Gilf Kebir Plateau (at G. Oweinat)...*". Their southern edge corresponds to the southern boundary of the area studied here (Fig. 1). Mohamed et al. (2017) also estimated a few millimetres per year of recharge for the Southern Kufrah basin. Voss and Soliman (2014) set a zero-infiltration rate for the period 5 ka BP until today. Conceptual approaches were also applied to the NSAS to identify the characteristic time scales of such large systems (e.g., Pallas 1980; Sonntag 1984, 1986; Bakhbakhi 2004; Vasseur et al. 2015). However, as the studies were built on conceptual models, recharge cannot be attributed to a specific area.

In conclusion, it remains unclear whether modern recharge occurs in northern Chad. The present investigation aims to assess the potential for modern recharge in the southern margins of the Kufrah basin in northern Chad, particularly the area between the oases of Faya-Largeau, the Ounianga Lakes and the Ennedi Mountains (Fig. 1). Specifically, this paper addresses the following questions:

1. Is there any potential for diffuse and/or concentrated infiltration in northern Chad?
2. Is there evidence that diffuse or concentrated infiltration contributes to groundwater recharge?

This study utilized (1) remote sensing data, and (2) analysis of chemical and stable isotopic composition of groundwater samples to assess recharge. By employing remote sensing data it was possible to assess the potential for diffuse and concentrated recharge through the period 2013–2016. For diffuse recharge, the potential is assessed by combining remotely sensed maps of precipitation (RFE2.0) and evapotranspiration (using Landsat 8). For concentrated recharge, its potential is assessed by monitoring the spatial and temporal extent of inundation along the wadis (using Landsat 8). Similar approaches were successfully applied in recent studies aimed at understanding the processes of modern diffuse and concentrated recharge in data-scarce arid and semiarid environments using remote sensing (i.e. Brunner et al. 2004; Khalaf and Donoghue 2012; Coelho et al. 2017; Sheffield et al. 2018; Ahmed and Shabana 2020). To elaborate on the extent to which these surface processes result in modern groundwater

recharge in the area studied here, field surveys focusing on the stable isotopic and hydrochemical parameters (major ions) were combined with the remote sensing images. Finally, measured hydraulic heads were qualitatively compared to the data of Ball (1927) and, in combination with the indication of active flow obtained through the isotopes and hydrochemistry, used as a possible indicator of modern recharge. The surveys were conducted in the framework of the ResEau-Tchad project (UNITAR 2016) between 2013 and 2016, covering an approximate area of 100,000 km^2.

Methods

Remote sensing

Remote sensing is applied to obtain the spatial and temporal patterns of precipitation, the extent of flooding in the wadis in response to precipitation, and evapotranspiration.

Precipitation

Within the available satellite products of rainfall estimates for the African continent (TRMM 3B42, CMORPH, TAMSAT, RFE 2.0, PERSIANN, ARC 2.0, CHIRPS, TARCAT), the African Rainfall Estimation Algorithm Version 2 (RFE 2.0) was selected because it covers the entire region in one raster map and does not have any data gaps. RFE 2.0 rasters were downloaded from the FEWS-NET data portal (FEWS-NET 2017) as 10-km-resolution monthly rainfall estimates from January 2013 to December 2016. The coordinate system of the rasters was first projected to the local coordinate system (UTM 34N) and monthly mean and annual precipitation estimates were prepared.

Inundation in response to precipitation

Landsat 8 was chosen because of its high spatial resolution and spectral capacities. The Landsat 8 platform collects image data for 9 shortwave spectral bands over a 190-km swath with a 30-m spatial resolution for all bands except the 15-m panchromatic band, and a TIRS sensor (TIRS = thermal infrared sensor), which collects image data for two thermal bands with a 100-m spatial resolution over a 190-km swath. The return period is 16 days. To cover the entire region and timeframe (2013–2016) of this investigation, a total of 448 images from 10 scenes were downloaded from the GloVis data portal (USGS 2017). These images were mostly acquired for the months of June to September (2013–2016), corresponding to the rainy season. Some additional images were acquired for March–May to assess the seasonal variability of perennial lakes, and from October–December to observe the persistence of inundation

along the wadis after the rainy season. Many of the available images have data gaps because of clouds. From the 448 images, 95 were of sufficient quality and without significant cloud cover and therefore could be used for further processing (surface runoff, evapotranspiration). All preprocessing and processing steps were performed in RStudio v. 1.1.463 and ArcMap 10.5.

The Normalized Difference Water Index (NDWI) proposed by McFeeters (1996) is a remotely sensed indicator for the presence of surface water. It is based on the difference in reflectance between the near-infrared (NIR) and the green bands. Modified versions of the classical NDWI are available, notably the MNDWI36 and MNDWI37 (Xu 2006), based on the difference in reflectance between the shortwave infrared-1 and -2 (SWIR1 and SWIR 2), respectively, and the green bands. MNDWI36 was employed as it appeared to be the most sensitive index to the conditions present in the project area.

$$\text{MNDWI36} = \frac{r_6 - r_3}{r_6 + r_3} \qquad (1)$$

where r_n ($n = 3, 6$) are the reflectance values of bands 3 and 6, respectively. MNDWI36 values range between -1 and $+1$. An area is flagged as inundated if the MNDWI36 is larger than 0.

Evapotranspiration

Since no readily available evapotranspiration maps such as the MOD16 products are available, evapotranspiration, therefore, had to be calculated based on available multispectral satellite images. A procedure based on the energy balance equation and the determination of an evaporative fraction expressing the "wetness" of a pixel, the S-SEBI procedure from Roerink et al. (2000) was applied to the 95 Landsat 8 images previously selected. The procedure on how daily evapotranspiration was calculated is summarized in section S1 of the electronic supplementary material (ESM). For a full description refer to Vogt (2019).

For the subsequent analysis, the daily evapotranspiration maps need to be upscaled to monthly values, and full areal coverage should be reached. This is somewhat challenging because of the large spatial extent of the study area and data gaps due to cloud coverage. Ten scenes acquired on different dates are necessary to cover the area of interest. While two images per month are acquired by Landsat 8, not all images are cloud or haze free. Only high-quality images were used, i.e. with no haze and clouds. The month presenting the best areal coverage and used in the following analysis is the month of August (2013–2016). Mean daily evapotranspiration rates were converted to monthly values by multiplying the number of days per month.

Effective rainfall (*P* – ET)

The difference between average precipitation (*P*) and evapotranspiration (ET) corresponds to a one-dimensional (1D) water balance across the soil surface, allowing one to identify patterns of potential recharge (Brunner et al. 2007). Note that the absolute values of this approach will be unreliable, given that both precipitation and evapotranspiration are uncertain. The uncertainties of the residual value are even higher because *P* and ET values are very close in arid and semiarid regions. Nevertheless, relative spatial and temporal differences can be identified through this approach.

To calculate the residual between *P* and ET, the maps need to have the same spatial resolution, and should also be from the same period. RFE2.0 precipitation rasters were resampled to the resolution of the monthly ET images obtained as described previously, and the residual (*P* – ET) was calculated for every month. As previously stated, the month of August (2013–2016) presented the best spatial coverage. The mean of the August monthly residuals for the years 2013–2016 is presented herein.

Field investigations

Sampling and measurements of hydraulic heads

Within the extent of the study area and in the neighbouring regions (Ennedi east, Lake Chad basin), a total of 143 localities with a water point were inspected in the field during three main field campaigns (January–February 2013, 2014 and 2015), covering ~100,000 km² (see Fig. 1 for the sampling location). Forty of these localities were inspected a second time during additional campaigns in July–August 2013 (Ennedi-Ounianga) and November–December 2016 (Ennedi). Measurements were taken mostly at wells and boreholes, but also at springs, lakes and ponds. All the most important perennial water points (lakes and springs) were sampled, while not all but a selection of boreholes or wells were sampled within the agglomerations (villages, oases). In 128 cases it was possible to measure the water table depth, and a total of 183 water samples were collected.

Water samples were filtered (anions, stable isotopes) and acidified with nitric acid (cations), then stored in HDPE and glass bottles in a portable refrigerator. The samples were analysed for major ions and stable isotopic contents at the University of Neuchâtel, Switzerland a few months after the sampling. Section S2 in the ESM provides the field observations (location, type, depth of the water point, water level depth; Table S2 in the ESM), the physico-chemical parameters and major ions (Table S3 in the ESM) and stable isotopes analysis (Table S4 in the ESM) of a selection of water sample locations. The complete dataset is available in Vogt (2019).

For the determination of the hydraulic heads, the depth to the water table was measured in boreholes and subtracted from topographic data extracted from the SRTM V4 dataset (Jarvis et al. 2008). The hydraulic heads of surface water features such as springs or lakes were associated with the elevation of these features and are likewise based on SRTM data.

Stable isotopes analysis

Stable isotopes ($\delta^{18}O$ and δ^2H, Table S4 in the ESM) were measured by cavity ring-down spectroscopy (Picarro L2140). Hydrogen and oxygen isotopes data are reported in terms of conventional delta (δ) notation and in units of per mill (‰) deviation relative to a standard reference:

$$\delta = \left[\frac{R_{\text{sample}}}{R_{\text{standard}}} - 1 \right] \times 10^3 \qquad (2)$$

where R corresponds to the isotopic ratio $R = {}^2H/{}^1H$, for deuterium, and $R = {}^{18}O/{}^{16}O$, for 18–oxygen, for both the sample and the standard. The standard used is the Vienna Standard Mean Ocean Water. The standard deviation of the analytical method is typically $\pm 1‰$ for δ^2H and $\pm 0.2‰$ for $\delta^{18}O$.

Major ions analysis and data treatment

Major ions were measured by ion chromatography (Dionex DX-120), whereby the uncertainty of the IC analysis is typically 5%. Quality assessment was performed by ionic balance calculation. Samples that were out of balance by >10% were discarded and are not shown herein (Table S3 in the ESM). In addition, alkalinity measurements were performed on filtered samples immediately after sampling. These measurements were used for cross-checking the validity of the bicarbonate analysis. For the determination of the water types, all concentrations are converted to % meq L^{-1} and all parameters above a threshold of 12.5% are included in the reported water types and are ordered according to their percentage: listing cations first, followed by the anions. When the element is indicated in parenthesis, that means that its concentration is not systematically higher than 12.5% meq L^{-1} for all the analysed samples, but is significantly enough represented to be indicated.

Results

Precipitation

In the study area, most, if not all, of the annual precipitation is linked to the summer monsoons occurring between mid-July and mid-September, with the highest rates being reached during the month of August. Annual differences are observable. 2014 was a particularly humid year, as opposed to the relatively dry year of 2016. Figure 2 shows the mean annual precipitation (2013–2016) in the study area. About 50% of the area considered in this study receives less than 50 mm year^{-1}. In the regions northwest of the Ennedi mountains (hereafter "the Ennedi"), precipitation varies between 5 (Gouro) and 25 mm year^{-1} (Ouanianga Kebir). Precipitation rates higher than 100 mm year^{-1} are found in the Ennedi mountains. Because the summer monsoons are SW-originating, the southern slopes of the Ennedi receive more precipitation than the northern slopes (orographic effect). Precipitation in the Erdis plateau is very low and the Tibesti mountains is receiving up 100 mm year^{-1}.

### Surface-water floodings in response to precipitation

The surface-water floodings (inundated surfaces) and their corresponding frequencies for August 2013, 2014, 2015 and 2016 are shown in Fig. 3. Note that the inundated surfaces are not to scale but were spatially enlarged by a factor of 50. This was done because otherwise the surfaces are too small to be visible on this spatial scale.

Inundated surfaces are essentially absent north of 20°N, increasing in extent and duration towards the more southern latitudes. Also, the extent of flooded areas increases in proximity to the mountainous regions. For the more western scenes, neighbouring the Tibesti mountains, maximum inundated surfaces reach 18.4 km^2, and 85.8 km^2 for the more eastern scenes, near the Ennedi mountains. Comparatively, maximum inundated surfaces in the central depressional areas reach only 4.6 km^2, meaning that the region of the Ennedi mountains can experience between 5 to 18 times more inundated surfaces than the rest of the concerned study area.

In terms of frequency of occurrence, all the main wadis of the southern slopes of the Ennedi, and Wadi Tebi for the northern slopes, are flooded every year (2013–2016), while in the eastern slopes of the Tibesti and the flat central regions, inundated surfaces are detected only once over the 4-year period inspected in this study. The inundated surfaces generally reach their maximum extent during August, constituting a short delay from the onset of the rainy season. The extent of the inundated surfaces decreases over September and generally disappears in October but can persist up to December for particularly humid years.

In particularly humid years, in this case, 2014, exceptional flows provoke large, inundated surfaces accumulating along the wadis. As an indication of the amplitude and importance of these episodic phenomena, surface water accumulating in August 2014 downstream of Wadi Tebi is ten times more extended than the perennial surface water of the whole group of lakes of Ounianga Serir (3.7 km^2 for Ounianga Serir, 36 km^2 for the area downstream of Wadi
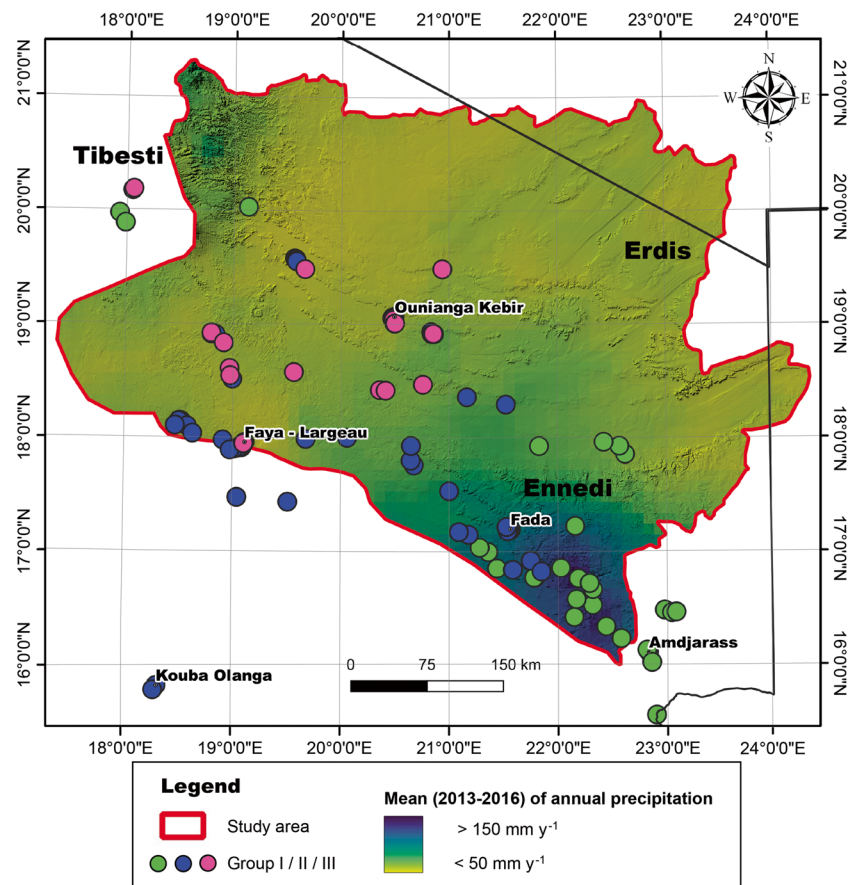
Tebi). The northern slopes of the Ennedi mountains receive <30 mm year^{-1} precipitation; nevertheless, runoff along Wadi Tebi is observable over an extent of up to 100 km. Essentially no inundated surfaces can be identified in the Erdis plateau.

Evapotranspiration

The month of August is particularly important because of the presence of extended flooded areas, corresponding therefore to the upper limit of evapotranspiration losses. The evapotranspiration map for the month of August (mean for 2013–2016, Fig. 4) shows that losses from evapotranspiration occur mainly (1) within the main discharge zones or oases (lakes, vegetation and subsurface water), and (2) within the alluvial systems of wadis. Daily actual evapotranspiration rates vary between 4 and 7 mm day^{-1} within the vegetated areas of the oases of Gouro, Bedo, Faya-Largeau, West Palm Groves, and the free water of the lakes of Ounianga Kebir and Serir. Daily actual evapotranspiration rates vary between 1 and 5 mm day^{-1} along the wadis.

From March to September (corresponding to the investigated period), monthly evapotranspiration rates are relatively stable for the oases. On the other hand, the flooded areas associated with the wadis show a significant increase

in evapotranspiration loss during the rainy season, progressively decreasing for some months. It is interesting to compare the relevant surface areas and the corresponding evapotranspiration to estimate the order of magnitude of loss for the oases and the wadis. The surface areas of the oases are: Ounianga Kebir, 22 km^2; Ouninaga Serir, 37 km^2; the oases of Gouro, 16 km^2; Bedo, 9 km^2; Faya-Largeau, 100 km^2; and the West Palm Groves (i.e. Aïn Galaka), 77 km^2. The associated annual loss through evapotranspiration ranges from 0.6 10^5 to 8.1 10^5 m^3 year^{-1}, depending on the surface extent of the oases, with a total of 2.2 10^6 m^3.

The total surface area of alluvial sediments along the wadis where evapotranspiration is detectable is 9,600 km^2. The cumulative volume of evapotranspiration losses occurring from June to September along the wadis is at least 10 times higher than the cumulated ET annual losses from the perennial lakes and oases.

Effective rainfall

The resulting map of (P – ET) for the month of August (mean 2013–2016) is used as a qualitative proxy for diffuse recharge (Fig. 5). In regions where surface runoff is important, such as along the wadis, the residual of (P – ET) is invariably negative because evapotranspiration rates are

Fig. 3 Inundated surfaces (MNDWI36 > 0) for August (2013–2016) over the study area and frequency of inundation occurrence (1, 2, 3, or 4 times in 4 years). The spatial scale of the inundated surfaces is exaggerated to ensure visibility. Groups I/II/III represent sampling locations. Their assignment is based on the isotopic analysis (see Fig. 6 for further explanation)
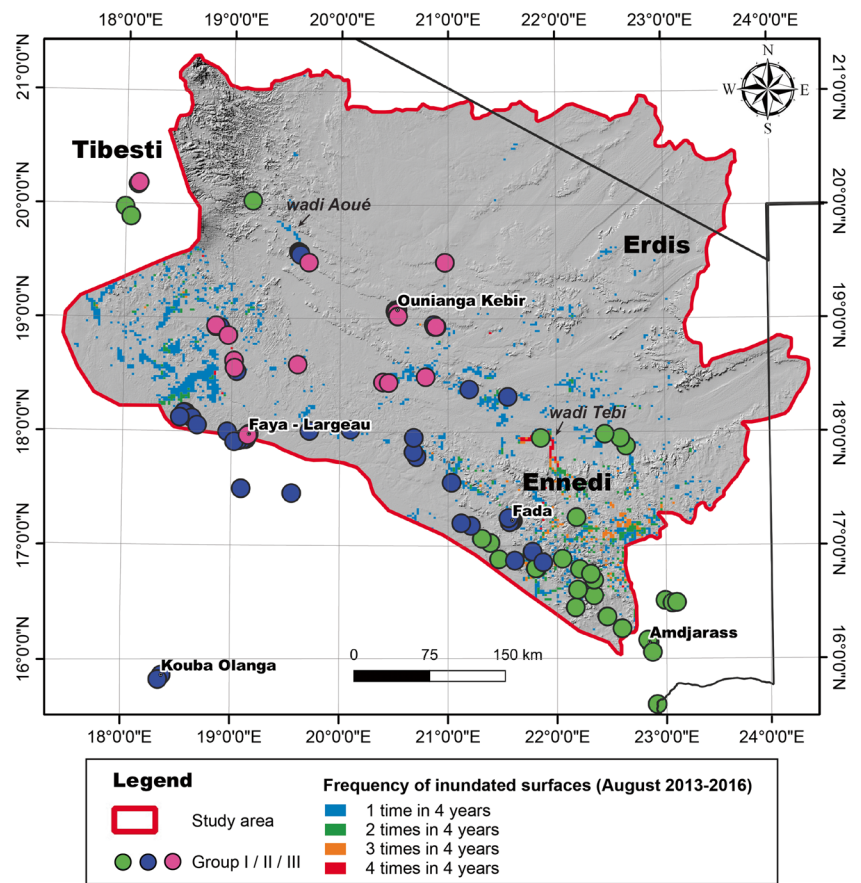
high for several months after the end of precipitation and flooding. The map shows an increased potential for diffuse recharge in the southern slopes and foothills of the Ennedi Mountains (shown in magenta in Fig. 5). Null or negative values are found in the areas where precipitation is less than 30 mm year^{-1}.

Hydraulic head

In the Ennedi mountains, the hydraulic heads are generally above 500 masl, while the main discharge zones (i.e. Ounianga) have generally hydraulic heads <500 masl. From the interpolated groundwater contours based on the field measurements (Fig. 5), it was deduced that from the southern and northern slopes of the Ennedi, groundwater flows first towards the WNW, then SW, whereas from the Tibesti, groundwater flows towards the SE and S, and in the central flat areas towards the SSW.

Hydraulic gradients derived from cross-sections are 3–4‰ in the Ennedi, while, within the SSW–NNE central flat zone, hydraulic gradients are 0.5–1‰. In the Ennedi mountains, the water-table depths vary from 0.1 to 1.3 m, with an exceptional maximum difference of 2.2 m between seasons. While only a few localities (three) were reinspected

a second time in the central flat regions, they all indicate no variation in the water-table depth.

Stable isotopes

The isotopic ratios of the groundwater samples from the 143 inspected localities and the 40 resampled localities vary between −11.7 and +20.1‰ $\delta^{18}O$ and between −85 and +91‰ δ^2H. Figure 6a shows the isotopic ratios of all the analysed samples. The data show that some of the groundwater was exposed to significant evaporation as indicated by an enrichment of heavy isotopes. These points are on the right of the meteoric water lines (white markers in Fig. 6a) and align along two distinct evaporation lines, named here Ennedi (ELE) and Ounianga Lake (OLEL) evaporation lines, given their geographical positions. They correspond to lakes, natural ponds, or abandoned open wells. The stable isotopic ratios of samples indicating evaporation vary between −6.6 and +20.1‰ $\delta^{18}O$ and between −61 and +91‰ δ^2H. Given that the focus here is on modern recharge, these points are only plotted in Fig. 6a, and not considered further.

The remaining nonevaporated samples plot along the Global Meteoric Water Line (GMWL) or parallel but slightly below, close to the Sahelo-Sudanese Meteoric

Fig. 4 Mean daily actual evapotranspiration for August (2013–2016). Grey zones indicate that no image was available for processing. Groups I/II/III represent sampling locations. Their assignment is based on the isotopic analysis (see Fig. 6 for further explanation)
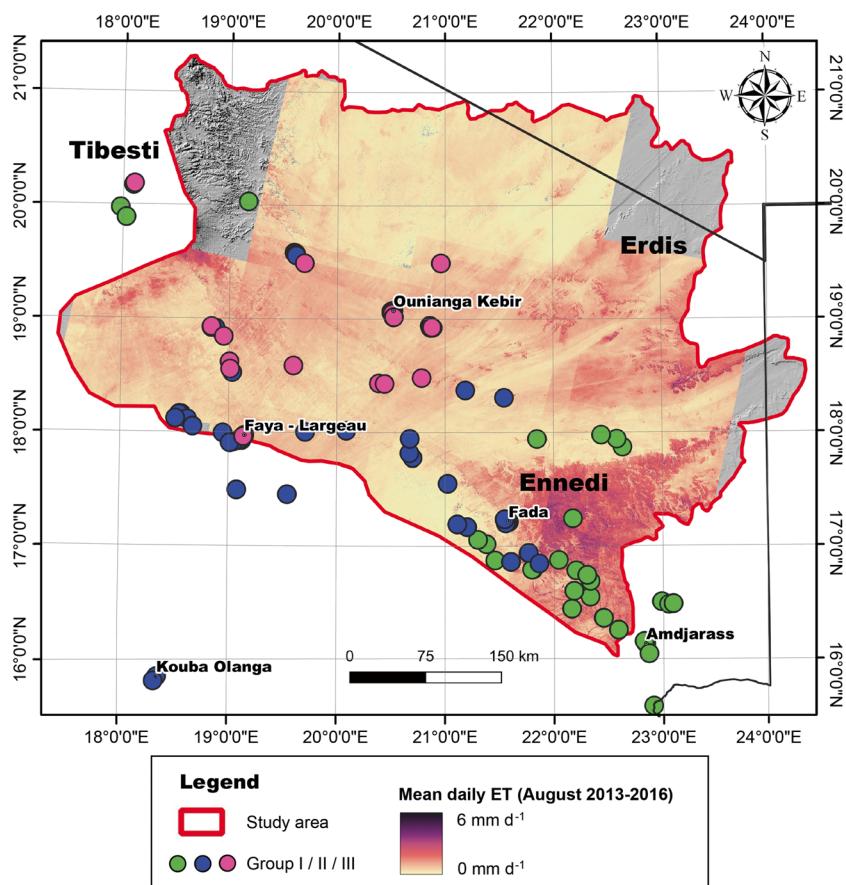
Water Line (SSMWL). Their stable isotopic ratios vary between –11.7 and –2.0‰ $\delta^{18}O$ and between –85 and –9‰ δ^2H. They were subdivided into groups. The isotopic signature of rainfall measured in Faya-Largeau is used for comparison. Group I was defined for the samples with the less depleted isotopic ratios (56 samples), which vary between –6.6 and –2.0‰ $\delta^{18}O$ and between –43 and –9‰ δ^2H. The isotopic ratios of group II (48 samples) were defined as the range between –8.9 and –5.9‰ $\delta^{18}O$ and between –68 and –42‰ δ^2H, while for group III (41 samples), the most depleted ones, stable isotopic ratios vary between –11.7 and –8.9‰ $\delta^{18}O$ and between –85 and –62‰ δ^2H. The spatial distributions of these groups are shown in Figs. 2, 3, 4, and 5.

The stable isotopic groups show interesting patterns in relation to the hydraulic heads and the precipitation rates, as illustrated in Fig. 6b,c (in this case $\delta^{18}O$ is shown). The most depleted samples (group III) are found in the central flat regions with hydraulic heads below 450 masl and precipitation rates below 40 mm year^{-1}. The less depleted samples (group I) are located in the Ennedi mountains with hydraulic heads above 450 masl and both higher precipitation rates (>50 mm year^{-1}), when located in the southern slopes, and lower precipitation rates (<40 mm year^{-1}), when located in the northern slopes (Mourdi Djouna to Tebi).

Major ions

The sampled groundwater shows generally a low to medium level of dissolved ion content (electrical conductivity (EC) between 20 and 665 µS cm^{-1}), and a pH between 6 and 9, whereas 12% of the samples show EC > 2,500 µS cm^{-1}. The lakes of Ounianga have the highest dissolved ion content within the collected samples (up to 196 mS cm^{-1}) and alkaline pH (pH 9.0–11.2).

In terms of the definition of water types, the main hydrochemical families are: Ca–(Mg)–HCO$_3$, Ca–(Mg)–Na–HCO$_3$, Na–Ca–(Mg)–HCO$_3$, and Na–HCO$_3$–(Cl–SO$_4$). Hydrochemical signatures showing a specific enrichment in K, NH$_4$, NO$_3$ or F were also found, but are not considered herein because they represent exceptions.

The chemical and stable isotopic distribution (Fig. 7) shows that the less depleted (group I) and depleted (group II) isotopic ratios are generally associated with samples with a similar hydrochemical signature, characterized by Ca–(Mg)–HCO$_3$ and Ca–(Mg)–Na–HCO$_3$ water types. The most depleted (group III) are associated with Na–Ca–HCO$_3$, Na–HCO$_3$ and Na–Mg–HCO$_3$ water types and higher contents of Cl and SO$_4$ (see the ESM).

The relationship between the samples' chemical composition and their stable isotopic signature is therefore expressed

Fig. 5 Representation of (P – ET) for August (mean 2013–2016). Given the large uncertainties of this residual, the absolute values are deliberately not indicated. The figure suggests that most of the area has a very low potential for diffuse recharge, except the southern slopes of the Ennedi mountains. The groundwater level contours and flow directions are derived from the water-table depth measurements performed in the field. Groups I/II/III represent sampling locations. Their assignment is based on the isotopic analysis (see Fig. 6 for further explanation). Boxes A, B, and C indicate the areas shown in Fig. 8
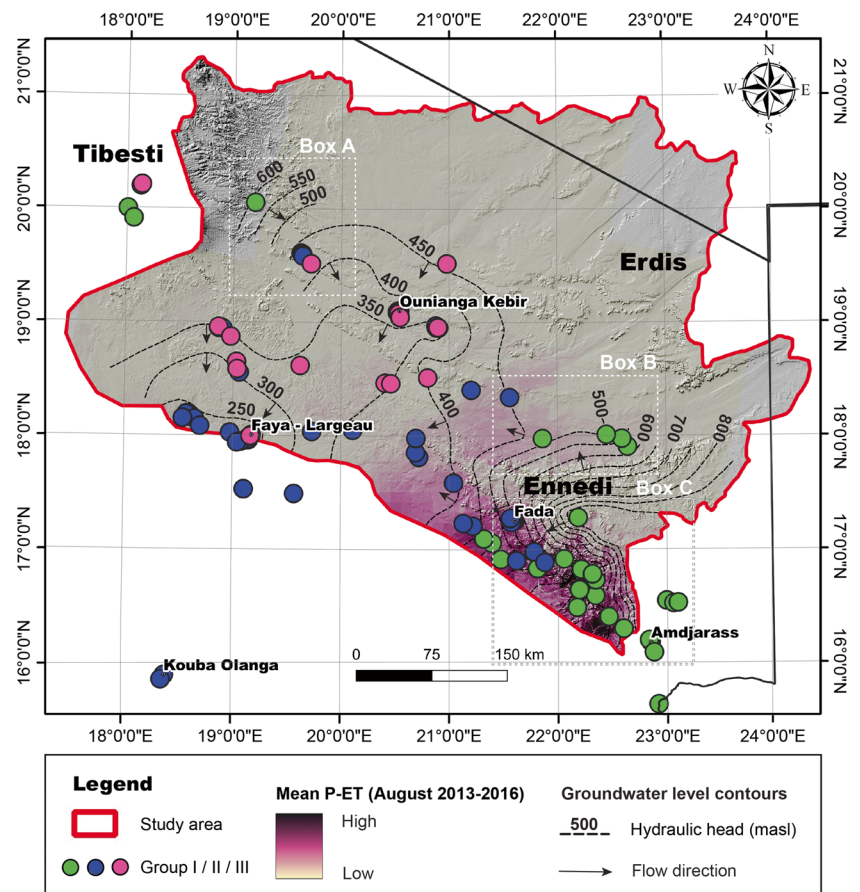
by the cation facies change from Ca–Mg-dominant (less depleted), through Ca–Na, Na–Ca to Na-dominant (most depleted, Fig. 7).

Discussion

The aim of this study was (1) to identify areas and mechanisms of potential modern recharge in the NSAS of northern Chad, and (2) to evaluate if this potential recharge contributes to groundwater recharge. Point (1) is entirely based on remote sensing data which provide crucial information concerning climatic and hydrologic dynamics. Point (2) is elaborated by combining the stable isotopic and chemical compositions of the groundwater with the areas of potential recharge. Also discussed is the hydraulic head as a possible indicator for modern recharge.

Indications for groundwater recharge based on the flowfield

There are two clear indications for groundwater flow in the region of the Ennedi: the hydraulic gradient values, and the evolution of the water chemistry. Concerning the

hydraulic gradient, it is interesting to compare the contour lines (see Fig. 1) obtained by Ball (1927) with the current ones (Fig. 5). While an exact comparison is not possible due to the absence of the raw data of Ball (1927), no obvious change in the flowfield can be identified. One could in principle argue that, given that a hydraulic gradient is present and there were no obvious changes in hydraulic head in the last 100 years, modern recharge must occur to maintain the general direction of the flowfield. While this can be seen as an indication of recharge, no definitive conclusions can be drawn based on this argument alone, for two reasons. As shown by Thorweihe and Heinl (2002), Gossel et al. (2004), Voss and Soliman (2014), and Vasseur et al. (2015), the characteristic time-scale of this system is on the order of thousands of years. A comparison with data obtained a hundred years ago is too short a period to conclude that modern recharge occurs. Another point that precludes hydraulic heads as a definitive indicator for modern recharge is that of unknown hydraulic properties. The hydraulic gradients could result in very small fluxes if the hydraulic conductivity of the system is very small. In summary, the obtained hydraulic head data do not exclude an interpretation of modern recharge, but, by themselves, such data are insufficient proof of modern recharge.
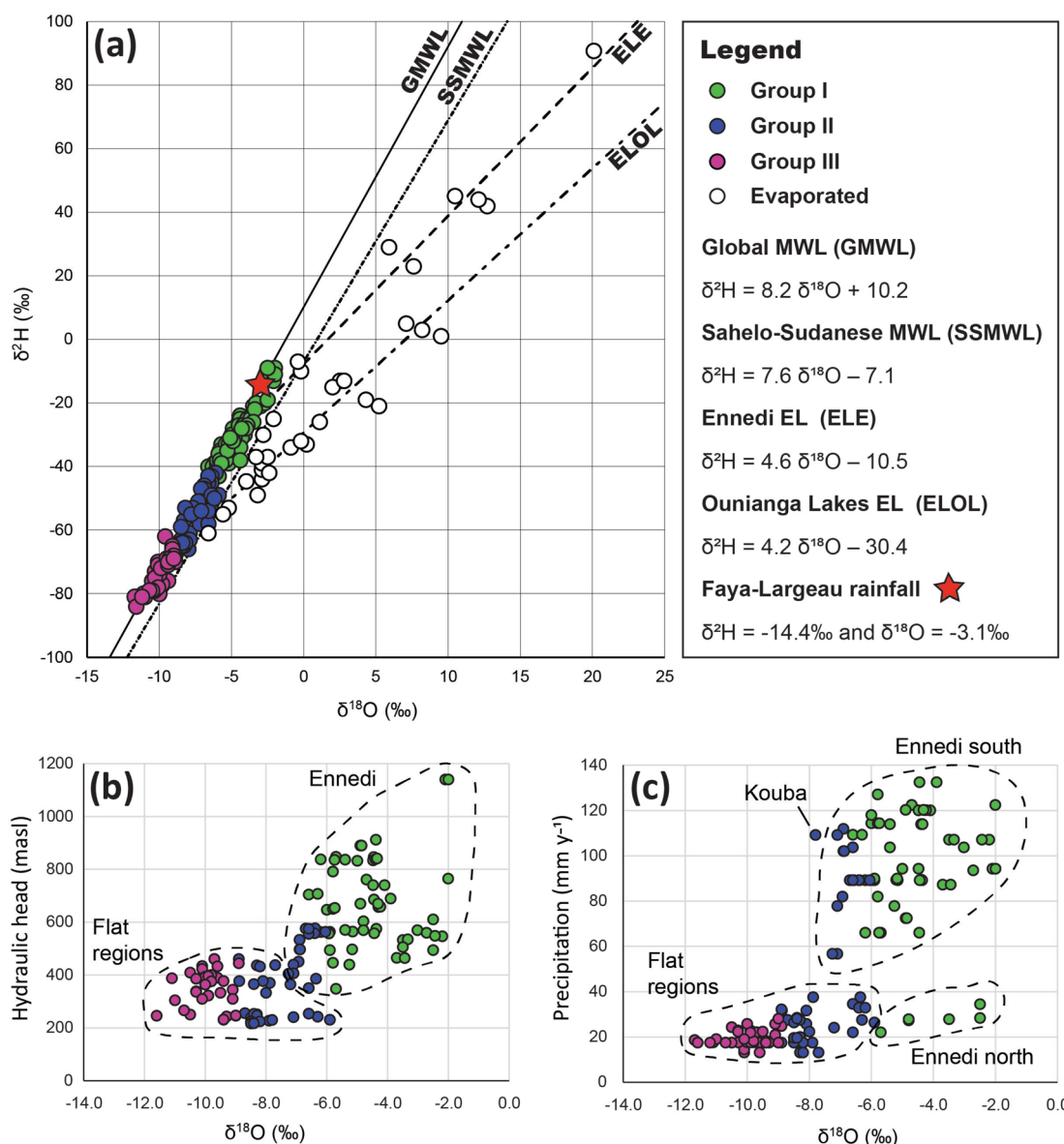
Fig. 6 **a** δ^2H versus $\delta^{18}O$ ratios. The samples are divided into evaporated and nonevaporated. The nonevaporated samples are subdivided into three groups. The lines correspond to the Global Meteoric Water Line (GMWL, $\delta^2H = 8.2\delta^{18}O + 10.2$, Craig 1961), the Sahelo-Sudanese Meteoric Water Line (SSMWL, $\delta^2H = 7.6\delta^{18}O - 7.1$, Joseph et al. 2012) and the calculated evaporation line for samples from the Ennedi mountains (ELE, $\delta^2H = 4.6\delta^{18}O - 10.5$) and from the Ounianga Lakes (ELOL, $\delta^2H = 4.2\delta^{18}O - 30.4$). The isotopic signature of

rainfall measured in Faya-Largeau (IAEA-GNIP database) is shown as a reference (red star). The enriched values (–3.3 to 0.5‰ $\delta^{18}O$ and –15 to 1‰ δ^2H, and three measurements in August 1968, July 1973 and August 1977) of Faya-Largeau's rainfall are comparable with the general isotopic content of current rains measured in Central and Northern Africa (Joseph et al. 2012; Sonntag et al. 1976, 1978). **b** Hydraulic head (masl) against $\delta^{18}O$ (‰). **c** Rainfall rate (mm year^{-1}) against $\delta^{18}O$ (‰). Only nonevaporated samples are shown (**b**–**c**)

Concerning the chemistry, there are, however, indications that there is a continuous flow of groundwater from the Ennedi mountains towards the central flat areas. In the mountainous areas, in correspondence to the zones of the highest potential for diffuse (Fig. 5) and concentrated recharge (Fig. 3), the chemical composition of groundwater varies between Ca–(Mg)–HCO₃ and Ca–(Mg)–Na–HCO₃, following the groundwater flow directions. This applies to

all the groundwater sampled in the Ennedi: the springs of Archeï and Bachiquele, the shallow groundwater of the oasis of Fada and the subsurface water from the alluvial systems of wadis (southern and northern slopes). Groundwater samples in flat areas (Faya-Largeau, Gouro, Ounianga) have higher concentrations of Na, Cl and SO₄. The groundwater hydrochemical type found in the higher zones of the Ennedi is compatible with the hydrochemical type of current
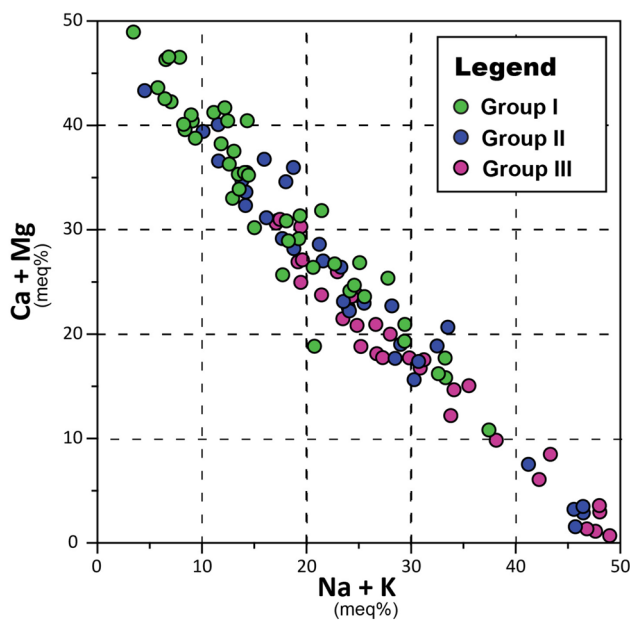
Fig. 7 Ca+Mg (meq%) vs. Na+K (meq%) showing the progressive cation facies change from Ca+Mg–dominant species (groups I and II) to Na+K-dominant species (group III). The different colours represent the different groups defined in section 'Stable isotopes'

rainfall, and the observed hydrochemical changes along the groundwater flow directions are compatible with an increase in residence time from the higher zones of the Ennedi to the lower zones of the oases (mainly cation exchange).

Potential diffuse and concentrated recharge

The comparison of precipitation and evapotranspiration data for the period 2013–2016 shows that precipitation rates are higher than the evapotranspiration rates only during August. While the absolute values of P and ET are highly uncertain, the results suggest that if diffuse recharge occurs, it will be in the southern part of the Ennedi mountains only; however, with the remote sensing data alone, no definitive conclusion can be shown.

Concerning concentrated recharge, spectacular floods occur every year, both within the southern and northern slopes of the Ennedi mountains, as well as in the southeastern Tibesti. The flooding remains long enough to capture the essential spatial and temporal dynamics of the inundation, despite the relatively long return period (16 days) of the Landsat 8 satellite. Inundated surfaces are initially large, then gradually recede for several months after the end of the rainy season (e.g., wadi Tebi). Total losses from evapotranspiration along the wadis are significantly larger (around one order of magnitude) than from the permanent free water and subsurface water in the oases. The periods of inundation do not necessarily match the period

of infiltration. During the stagnant period of inundation, colmation can occur, which might reduce the infiltration capacity of the underlying soil. As for the diffuse recharge, the remote sensing cannot provide conclusive proof that the potential recharge translates into actual recharge. The next section combines isotopic data with remote sensing to tackle this question.

Indications for modern recharge vs. paleorecharge

The key to differentiating modern recharge from paleorecharge (fossil groundwater) is the isotopic data, and to a certain extent the chemical composition as well. Groundwater samples with enriched isotopic ratios ($\delta^{18}O > -4.9‰$) are comparable with the current precipitation in terms of stable isotopic signature. These sampling locations are located in the southern Ennedi, in correspondence with the zone of highest potential for diffuse recharge, and within the alluvial systems of wadis that are episodically flooded.

Groundwater samples with depleted isotopic ratios ($\delta^{18}O < -8‰$) originate from sampling points in the central flat areas with very little precipitation. This signature is comparable with similar compositions found in samples from oases and sabkhas in Libya (Goudarzi 1970; Pachur and Altmann 2007) and in the Lake Chad basin (Herrmann et al. 2009), and are associated with groundwater recharged during the Pleistocene-Holocene. Ages of 9,600–7,500 years were determined for groundwater of Faya-Largeau, with associated $\delta^{18}O$ ratios varying between –9 and –10.5‰ (Schneider 1989). Poulin (2019) estimated an age of 10,000 years for the Ounianga Lakes with ^{14}C analyses, in accordance with their depleted isotopic ratio measured in this study.

This interpretation is also consistent with the hydrochemical data. Samples depleted in heavy isotopes are generally of the Na–HClO$_3$–(Cl–SO$_4$) type, which can be explained by the high residence time in the sandstone aquifers leading to ion-exchange and slow silicate weathering releasing Na$^+$. In contrast, samples with an enriched isotopic signature ($\delta^{18}O > -4.9‰$) tend to have a higher plroportion of Ca^{2+} and Mg^{2+}. Analogous trends were also observed in other zones of the NSAS. Hesse et al. (1987) observed distinct hydrochemical zones for groundwater of the Dongola area of Egypt: groundwater strongly influenced by the infiltrating River Nile water had dominantly a Ca–Mg–HCO$_3$ type, evolving towards an increased content of Na, SO$_4$ and Cl for deep and shallow wells away from the river. Wright et al. (1982) observed an increase of Na+K and SO$_4$ contents over Ca+Mg and HCO$_3$ along the flow lines for groundwater from the Kufrah subbasin. These same trends are observed in northern Chad.
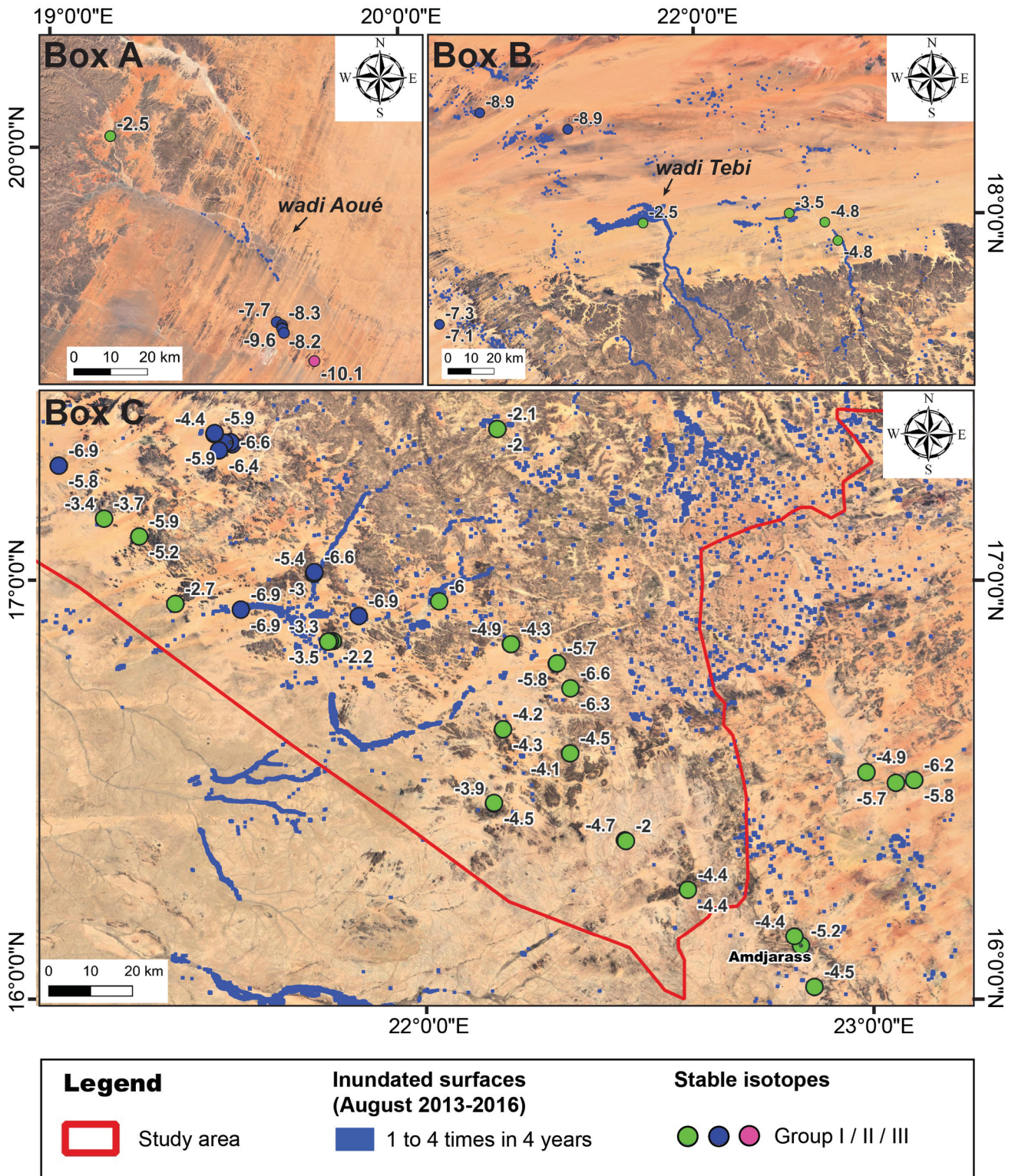
Fig. 8 Overlay of the different isotopic groups with the inundated surface (see also Fig. 3) for box A the southeastern Tibesti mountains, box B the northern Ennedi mountains, and box C the southern Ennedi mountains. The background images were obtained from Google Earth

Indications for the mechanisms of modern recharge

While the isotopic data are a robust indicator for modern recharge, the dominant recharge mechanism (diffuse vs. concentrated recharge) can be best elaborated by combining the remote sensing data with the spatial location of the different groups. In principle, in areas where the potential for diffuse recharge is essentially null, group III is the dominant group, indicating that no modern recharge is occurring (Fig. 5). Nevertheless, several points (e.g. in the north of the Ennedi and in the southeast of the Tibesti) clearly indicate modern recharge despite the small potential for diffuse recharge. Figure 8 shows a zoom to these areas, plotting the different groups jointly with the inundated surfaces.

The data clearly suggest that the dominant recharge mechanism for modern recharge in areas with very small diffuse recharge is through concentrated recharge. Starting with the Tibesti (Fig. 8, box A) one sample of group I, corresponding to a similar composition to the current precipitation in the region, is found close to the mountains, while further downstream, groups II and III are dominant, clearly indicating the spatial extent of concentrated recharge. North of the Ennedi mountains the situation is very similar (Fig. 8, box B). Given that the potential for diffuse recharge is essentially null, concentrated recharge is the dominant mechanism in these areas. South of the Ennedi (Fig. 8, box C), the remotely sensed maps of potential diffuse recharge, as well as the presence of periodically flooded wadis, indicate that both concentrated and diffuse recharge can occur concurrently.

While no samples were obtained from the Erdis region, the potential for diffuse recharge is very low, and no observable inundations occur. It is not expected that there will be any significant contribution of modern recharge in this region.

Conclusions

This study aims to assess whether modern recharge occurs in the Nubian Sandstone Aquifer System of northern Chad, and if so through which processes. From a methodological point of view, this study area presents particular challenges, as it is very large and difficult to access. So far, results from only a few studies in this region are available. Through the combination of spatially exhaustive remote sensing data (providing insights concerning surface-related processes) with hydrochemical, stable isotopic and piezometric data, a link between surface processes and recharge mechanisms could be established. The following conclusions concerning modern recharge in northern Chad can be developed.

Despite its extreme aridity, modern recharge occurs in northern Chad. It occurs both through concentrated infiltration through the wadis and through diffuse infiltration. Although this study does not provide the absolute value of recharge of the two mechanisms, by considering the spatial and temporal components of the two different recharge types, concentrated recharge can be defined as the most prominent and effective mechanism of recharge in northern Chad.

The only area where diffuse recharge potentially occurs is in the south of the Ennedi mountains. Given that precipitation is concentrated mostly in August, it is unlikely that diffuse recharge occurs during other periods of the year. No diffuse recharge is expected in the northern Ennedi, southeast Tibesti, central flat areas and in the Erdis regions.

For the southeast Tibesti and the area north of the Ennedi mountains, the only recharge mechanism is through concentrated recharge along the episodically flooded wadis, while south of the Ennedi, diffuse and concentrated recharge occur concurrently during the month of August. The inundated surfaces persist up to 3 months after the precipitation ceases, as opposed to diffuse infiltration processes which essentially are finished after the end of precipitation. As shown by the frequency of occurrence, the period of the inundated surfaces varies significantly from year to year.

Proof that modern recharge occurs within the Ennedi Mountains of northern Chad is particularly important for this arid region. However, given the limited recharge rates and the anticipated effects of climate change, it is vital to conduct quantitative assessments using ground-based monitoring data to ensure informed decision-making for the sustainable management of this resource. Several unique and fragile ecosystems depend entirely on this modern recharge, such as the Archeï and Bachiquele springs in the Ennedi Mountains. At the same time, little is known about the significance of this modern recharge to the transboundary NSAS. According to the general representation of the NSAS, the mountainous areas of northern Chad and northern Sudan are critical to the entire system. However, the regional piezometric dome highlighted by previous authors cannot be explained by modern recharge in northern Chad, given the latter's limited extent both in time and space. Other explanations, in particular a combination of the inertia of the aquifer system and paleorecharge, are therefore preferred.

Declarations

Conflict of interest On behalf of all authors, the corresponding author states that there are no conflicts of interest.

References

Abouelmagd A, Sultan M, Milewski A, Kehew AE, Sturchio NC, Soliman F, Krishnamurthy RV, Cutrim E (2012) Toward a better understanding of palaeoclimatic regimes that recharged the fossil aquifers in North Africa: inferences from stable isotope and remote sensing data. Palaeogeogr Palaeoclimatol Palaeoecol 329:137–149

Ahmed AA, Shabana AR (2020) Integrating remote sensing, GIS and geophysical data for recharge potentiality evaluation in Wadi El Tarfa, Eastern Desert, Egypt. J Afr Earth Sci 172. https://doi.org/10.1016/j.jafrearsci.2020.103957

Bakhbakhi M (2004) Hydrogeological framework of the Nubian Sandstone Aquifer System. In: Appelgren B (ed) Managing shared aquifer resources in Africa. ISARM-Africa, IHP-VI, Series on Groundwater no. 8. UNESCO, Paris, pp 177–201

Ball J (1927) Problems of the Libyan desert. Geogr J 70:21–38

Brunner P, Bauer P, Eugster M, Kinzelbach (2004) Using remote sensing to regionalize local precipitation recharge rates obtained from the chloride method. J Hydrol 294(4):241–250. https://doi.org/10.1016/j.jhydrol.2004.02.023

Brunner P, Hendricks Franssen H-J, Kgotlhang L, Bauer-Gottwein P, Kinzelbach W (2007) How can remote sensing contribute in groundwater modeling? Hydrogeol J 15:5–18

CEDARE (2002) Regional Strategy for the Utilization of the Nubian Sandstone Aquifer System. Volume II. CEDARE, Heliopolis Bahry, Cairo, Egypt

Coelho VHR, Montenegro S, Almeida CN, Silva BB, Oliveira LM, Gusmão ACV, Freitas ES, Montenegro AAA (2017) Alluvial groundwater recharge estimation in semi-arid environment using remotely sensed data. J Hydrol 548:1–15. https://doi.org/10.1016/j.jhydrol.2017.02.054

Craig H (1961) Isotopic variations in meteoric waters. Science 133:1702–1703. https://doi.org/10.1126/science.133.3465.1702

Edmunds WM (2009) Palaeoclimate and groundwater evolution in Africa: implications for adaptation and management. Hydrol Sci J 54:781–792

Edmunds WM, Wright EP (1979) Groundwater recharge and palaeoclimate in the Sirte and Kufra basins, Libya J Hydrol 40:215–241. https://doi.org/10.1016/0022-1694(79)90032-5

El Bakri A, Tantawi A, Blavoux B, Dray M (1991) Sources of water recharge identified by isotopes in El Minya Governorate (Nile Valley, Middle Egypt). IAEA, Vienna

FEWS-NET (2017) Monitoring & forecasting acute food insecurity. Famine Early Warning Systems Network. https://www.fews.net. Accessed Dec 2017

Gossel W, Ebraheem AM, Wycisk P (2004) A very large scale GIS-based groundwater flow model for the Nubian sandstone aquifer in Eastern Sahara (Egypt, northern Sudan and eastern Libya). Hydrogeol J 12:698–713. https://doi.org/10.1007/s10040-004-0379-4

Goudarzi GH (1970) Geology and mineral resources of Libya: a reconnaissance. US Gov Printing Office, Washington, DC

Heinl M, Brinkmann PJ (1989) A groundwater model of the Nubian aquifer system. Hydrol Sci J 34:425–447. https://doi.org/10.1080/02626668909491350

Herrmann L, Mounkaila M, Graef F (2009) Are there valuable pedological palaeoenvironmental indicators in Northern Chad? In: Holocene palaeoenvironmental history of the Central Sahara. CRC, Boca Raton, FL, pp 129–148

Hesse KH, Hissene A, Kheir O, Schnacker E, Schneider M, Thorweihe U (1987) Hydrogeological investigations in the Nubian Aquifer system, Eastern Sahara. In: Kilitzsch E, Schranck E (eds) Research in Egypt and Sudan. Reimer, Berlin, pp 397–464

Jarvis A, Reuter HI, Nelson A, Guevara E (2008) Hole-filled seamless SRTM data V4. Tech. Report, International Centre for Tropical Agriculture, Palmira, Colombia

Joseph A, Frangi JP, Aranyossy JF (2012) Isotope characteristics of meteoric water and groundwater in the Sahelo-Sudanese zone. J Geophys Res Atmos 97:7543–7551. https://doi.org/10.1029/92JD00288

Khalaf A, Donoghue D (2012) Estimating recharge distribution using remote sensing: a case study from the West Bank. J Hydrol 414–415:354–363

Klitzsch E, Sonntag C, Weistroffer K, Shazly EME (1976) Grundwasser der Zentralsahara: fossile vorräte [Groundwater of the Central Sahara: fossil reserves]. Geol Rundsch 65:264–287. https://doi.org/10.1007/BF01808466

Mahamoud AH (1986) Geologie und Hydrogeologie des Erdis-Beckens, NE-Tschad [Geology and Hydrogeology of the Erdis Basin, NE Chad]. Reimer, Berlin

McFeeters SK (1996) The use of the Normalized Difference Water Index (NDWI) in the delineation of open water features. Int J Remote Sens 17:1425–1432. https://doi.org/10.1080/01431169608948714

Mohamed A, Sultan M, Ahmed M, Yan E, Ahmed E (2017) Aquifer recharge, depletion, and connectivity: inferences from GRACE, land surface models, and geochemical and geophysical data. GSA Bull 129:534–546. https://doi.org/10.1130/B31460.1

Muller AB, Haynes CVJ (1984) Isotope hydrology of the shallow groundwaters of the western desert. Isot Hydrol 1983 Proc Symp, Vienna, September 1983

Münnich KO, Vogel JC (1963) Untersuchungen an pluvialen Wässern der Ost-Sahara [Studies on pluvial waters of the Eastern Sahara]. Geol Rundsch 52:611–624. https://doi.org/10.1007/BF01821145

ORSTOM (1962) Etudes d'hydrologie superficielle en régions sub-désertiques et désertiques d'Afrique Noire [Surface hydrology studies in subdesert and desert regions of Black Africa]. Terres Eaux 38:46–73

Pachur H-J, Altmann N (2007) Die Ostsahara im Spätquartär: Ökosystemwandel im größten hyperariden Raum der Erde [The Eastern Sahara in the late Quaternary: ecosystem change in the largest hyperarid region on Earth]. Springer, Heidelberg, Germany

Pallas P (1980) Water resources of the Socialist People's Arab Libyan Republic. Proc. of the Second Symposium on the Geology of Libya, Academic, London

Poulin C (2019) Bilans hydrologiques et étude de la recharge de trois systèmes lac-aquifère du Bassin du Lac Tchad par une approche géochimique multi traceurs (δ18O, δ2H, 36Cl, 14C). [Hydrological balances and study of the recharge of three lake-aquifer systems in the Lake Chad Basin using a multi-tracer geochemical approach (δ18O, δ2H, 36Cl, 14C)]. PhD Thesis, Centre Européen de Recherche et d'Enseignement des Géosciences de l'Environnement, Universite d'Aix Marseille, France

Roerink GJ, Su Z, Menenti M (2000) S-SEBI: a simple remote sensing algorithm to estimate the surface energy balance. Phys Chem Earth Part B: Hydrol Oceans Atmos 25(2):147–157. https://doi.org/10.1016/S1464-1909(99)00128-8

Said MM, El-Mehdi B (2000) Jabal Asbah NF 35-1. Joint geological mapping project 1:250′000. Geol Surv Egypt and Industrial Res. Centre, Tajoura, Libya

Schneider J-L (1989) Géologie et Hydrogéologie de la république du Tchad [Geology and Hydrogeology of the Republic of Chad]. Masson, Paris

Sefelnasr A, Gossel W, Wycisk P (2015) Groundwater management options in an arid environment: The Nubian Sandstone Aquifer System, Eastern Sahara. J Arid Environ 122:46–58. https://doi.org/10.1016/j.jaridenv.2015.06.009

Sheffield J, Wood EF, Pan M, Beck H, Coccia G, Serrat Capdevila A, Verbist K (2018) Satellite remote sensing for water resources management: potential for supporting sustainable development in data-poor regions. Water Resour Res 54:9724–9758. https://doi.org/10.1029/2017WR022437

Sonntag C (1984) Autochthonous groundwater in the confined Nubian Sandstone aquifers. Berliner Geowiss Abh 50:217–220

Sonntag C (1986) A time-dependent groundwater model for the Eastern Sahara. Berliner Geowiss Abh 72:124–134

Sonntag C, Neureuther P, Kalinke C, Münnich KO, Klitzsch E, Weistroffer K (1976) Zur Paläoklimatik des Sahara: Kontinentaleffekt im D- 18O-Gehalt pluvialer Saharawässer [On the paleoclimate of the Sahara: continental effect in the D-18O content of pluvial Saharan waters]. Naturwissenschaften 63:479–479

Sonntag C, Klitzsch E, Loehnert EP, El Shazly EM, Münnich KO, Junghans C, Thorweihe U, Weistroffer K, Swailem FM (1978) Paleoclimatic information from D and 18O in 14C-dated North Saharian groundwaters: groundwater formation in the the past. Isotope Hydrology, Vienna, IAEA: 569–580

Sonntag C, Thorweihe U, Rudolph J (1982) Isotopenuntersuchungen zur Bildungsgeschichte saharischer Palaowasser [Isotope studies on the formation history of Saharan paleowater]. Geomethodica 7:55–78

Sturchio NC, Arehart GB, Sultan M, Sano Y, AboKamar Y, Sayed M (1996) Composition and origin of thermal waters in the Gulf of Suez area. Egypt Appl Geochem 11:471–479. https://doi.org/10.1016/0883-2927(96)00025-X

Suckow A, Sonntag C, Grönig M, Thorweihe U (1993) Ground water recharge in Umm Kedada Basin, NW-Sudan, derived from environmental isotopes of soil moisture in samples collected from deep dug wells. In: Schandelmeier H, Thorweihe U (eds) Geoscientific research in Northeast Africa. CRC, Boca Raton, FL, pp 677–685

Sultan M, Sturchio N, Hassan FA, Hamdan MAR, Mahmood AM, Alfy ZE, Stein T (1997) Precipitation source inferred from stable isotopic composition of pleistocene groundwater and carbonate deposits in the Western Desert of Egypt. Quat Res 48:29–37. https://doi.org/10.1006/qres.1997.1907

Swailem FM, Hamza MS, Aly AIM (1983) Isotopic composition of groundwater in Kufra, Libya. Int J Water Resour Dev 1:331–341

Thorweihe U, Heinl M (2002) Groundwater resources of the Nubian Aquifer System NE Africa. Observatoire du Sahara et du Sahel, Paris

UNITAR (2016) ResEau-Tchad project. United Nations Institute for Training and Research. http://www.reseau-tchad.org. Accessed Dec 2016

USGS (US Geological Survey) (2017) Welcome to GloVis. https://glovis.usgs.gov/. Accessed Dec 2017

Vasseur G, Rousseau-Gueutin P, de Marsily G (2015) Time constant of hydraulic-head response in aquifers subjected to sudden recharge change: application to large basins. Hydrogeol J 23:915–934. https://doi.org/10.1007/s10040-015-1252-3

Vogt M-L (2019) Contributions to the hydrology and hydrogeology of the Nubian Sandstone Aquifer System of Northern Chad. PhD Thesis, Center for Hydrogeology and Geothermics, University of Neuchâtel, Switzerland, 254 pp

Voss CI, Soliman SM (2014) The transboundary non-renewable Nubian Aquifer System of Chad, Egypt, Libya and Sudan: classical groundwater questions and parsimonious hydrogeologic analysis and modeling. Hydrogeol J 22:441–468. https://doi.org/10.1007/s10040-013-1039-3

Vrbka P, Thorweihe U (1993) Hydrogeology of the Wadi El Milk – Wadi Muqaddam area, northern Sudan. In: Schandelmeier H, Thorweihe U (eds) Geoscientific research in Northeast Africa. CRC, Boca Raton, FL, pp 693–698

Williams JJ (1966) South-Central Libya and Northern Chad: a guidebook to the geology and prehistory. Petroleum Exploration Society of Libya, Tripoli, Libya

Wright EP, Benfield AC, Edmunds WM, Kitching R (1982) Hydrogeology of the Kufra and Sirte basins, eastern Libya. Q J Eng Geol Hydrogeol 15:83–103. https://doi.org/10.1144/GSL.QJEG.1982.015.02.02

Xu H (2006) Modification of normalised difference water index (NDWI) to enhance open water features in remotely sensed imagery. Int J Remote Sens 27:3025–3033. https://doi.org/10.1080/01431160600589179